Flow Solvers," *Progress in Aerospace Sciences*, Vol. 36, No. 5–6, 2000, pp. 351–392.

[7]Dubuc, L., Cantariti, F., Woodgate, M., Gribben, B., Badcock, K. J., and Richards, B. E., "Solution of the Euler Unsteady Equations Using Deforming Grids," *AIAA Journal*, Vol. 36, No. 8, 1998, pp. 1417–1424.

[8]Harder, R. L., and Desmarais, R. N., "Interpolation Using Surface Splines," *Journal of Aircraft*, Vol. 9, No. 2, 1972, pp. 189–191.

[9]Girodroux-Lavigne, P., Grisval, J. P., Guillemot, S., Henshaw, M., Karlsson, A., Selmin, V., Smith, J., Teupootahiti, E., and Winzell, B., "Comparative Study of Advanced Fluid-Structure Interaction Methods in the Case of a Highly Flexible Wing (Results from the UNSI Program)," International Forum Aeroelasticity Structural Dynamics, Confereration of European Aerospace Societies/AIAA/Asociancion Espanola de Ingenieros Aeronauticos, June 2001.

[10]Yates, E. C., "AGARD Standard Aeroelastic Configurations for Dynamic Response I: Wing 445.6," Rept. 765, AGARD, 1988.

[11]Brown, S. A., "Displacement Extrapolation for CFD and CSM Analysis," AIAA Paper 97-1090, April 1997.

E. Livne
Associate Editor

Vortex Interaction of a Delta-Wing Flowfield

C. Shih* and Z. Ding†
Florida A&M University and Florida State University, Tallahassee, Florida 32310

Introduction

FOR the past several decades aspects of flows over delta wings, especially phenomena associated with leading-edge vortices, have been studied extensively.[1–7] At moderate angles of attack, the delta-wing flowfield is dominated by the presence of a pair of well-organized leading-edge vortices, commonly known as the primary vortices. Underneath the primary vortex the outboard-moving boundary layer separates as it approaches the leading edge to form a counter-rotating secondary vortex. Based on the averaged flow measurements, the secondary vortex is relatively small in size and peak magnitude as compared to the primary vortex. Additionally, its close proximity to the surface and the leading-edge shear layer makes it hard to be measured or computed accurately. These factors frequently lead to the conclusion that the secondary vortex only plays a secondary role and can be neglected in the delta-wing analysis. This characterization, however, has been challenged recently because it has been shown both experimentally[8,9] and numerically[10,11] that the interaction between the primary and the secondary vortices can be important in consideration of the overall flow behavior. The present experimental study examines in detail this interaction and its contribution to the unsteady characteristics of the entire flowfield. In this work we carried out experiments using particle image velocimetry (PIV) to study the leading-edge vortex flow over a delta wing. Our main objective is to explore the role played by the secondary vortex including its interaction with the primary vortex and its influence on the global vortex dynamics of the flowfield.

Experimental Setup

The experiments were carried out in a water towing tank facility. The delta wing has a leading-edge sweep angle of 60 deg and a root chord length of 13.0 cm. The experimental Reynolds number, based on the root chord length and the towing velocity, was 9.8×10^3. Both sides of the leading edge are sharp and beveled 45 deg leeward. The delta wing was set at an angle of attack of 12.5 deg. Detailed description of the experiment can be found in a previous paper.[8] The focus of the current study was on the detailed characterization of the unsteady motions of the leading-edge vortex flowfield using PIV technique. An 18-W argon-ion laser beam was expanded into pulsed laser sheets using a 24-faceted rotating mirror for image illumination. Tracer particles used were 10-μm silver-coated hollow glass beads with a specific gravity of 1.3. The PIV images were digitized by an optical scanner from 35-mm film images. The maximum error of the PIV technique in acquiring the instantaneous velocity and vorticity data was estimated to be 1 and 5%, respectively. More detailed discussions of the PIV technique can be found in the literature.[12,13]

Results and Discussion

To gain quantitative understanding of the behavior of the leading-edge vortex system, PIV measurements are taken along several crossflow planes that are normal to the freestream. Located on these planes, the y and z coordinates are defined, respectively, as the cross-stream and the span-wise directions, with their origin fixed at the left-side leading edge (as viewed from the trailing edge). In the discussions that follow, solid lines in the vorticity contour plots denote positive (clockwise) vorticity, whereas dashed lines denote negative (counterclockwise) vorticity. A time-averaged vorticity plot at a representative crossflow plane (50% chord, $x/C = 0.5$) is shown in Fig. 1. It can be seen that the primary vortex (solid lines) is well defined with a coherent vortex core. Located close to the leading edge and directly underneath the primary vortex, there exists the counter-rotating secondary vortex (dashed lines), which has a smaller amplitude as compared with the primary vortex. A strong shear layer emerges further outboard at the leading edge; high-amplitude vortical eddies can be observed to appear along the shear layer.

Figure 2 shows a representative sequence of the instantaneous primary/secondary vortex interaction at $x/C = 0.5$. The first frame is taken to be the reference time $t^+ = tU_\infty/C = 0.0$ (Fig. 2a) when the elongated primary vortex is tightly connected to the separating shear layer, allowing a continuous feeding of the shear layer vorticity into the primary vortex. During the next two instants (Figs. 2b and 2c), several individualized vortical eddies inside the primary vortex appear to roll up and coalesce into a highly concentrated vortical structure. Moreover, the secondary vortex is lifted upward to penetrate into the separating shear layer to sever the linkage between the primary vortex and the shear layer. In Fig. 2d, $t^+ = 0.384$, the shear layer appears to reconnect back to the primary vortex, and its primary vortical structure bears a close resemblance to the vortical structure in Fig. 2a, indicating the completion of a full interaction cycle. Through the analysis of a sequence of instantaneous PIV vorticity fields, it is observed that the interaction process indeed repeats itself in a quasi-periodic manner. Careful investigation of the interaction sequence reveals that each cycle consists of the following four repetitive stages: primary vortex induction/secondary vortex ejection, effect of the ejection process on the primary vortex, weakening of both the primary and secondary vortices, and reconnection of the primary vortex and the shear layer.

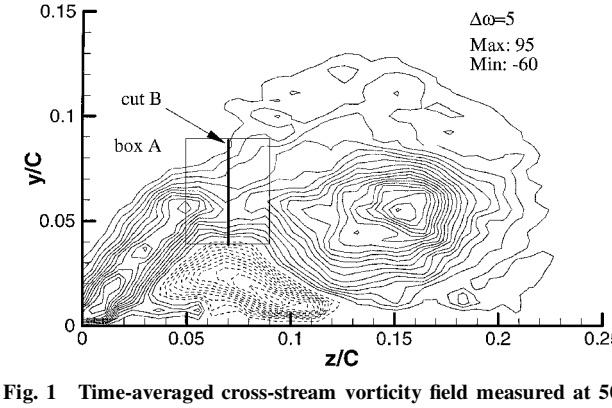

Fig. 1 Time-averaged cross-stream vorticity field measured at 50% chord.

Received 11 July 2000; revision received 10 September 2002; accepted for publication 19 September 2002.

*Professor, Department of Mechanical Engineering. Associate Fellow AIAA.

†Graduate Research Assistant, Department of Mechanical Engineering; currently Research Scientist, Exxon Mobil Upstream Research Company, Houston, TX 77252.

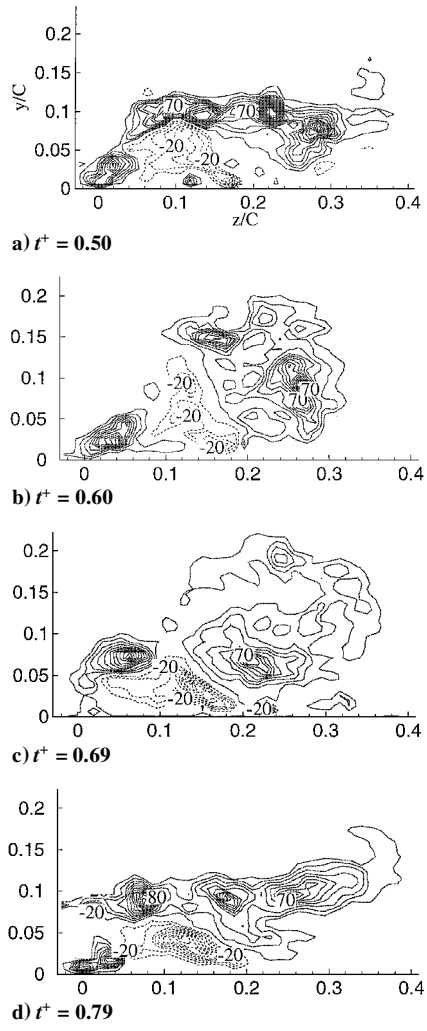

Fig. 2 Instantaneous cross-stream vorticity fields measured at 50% chord.

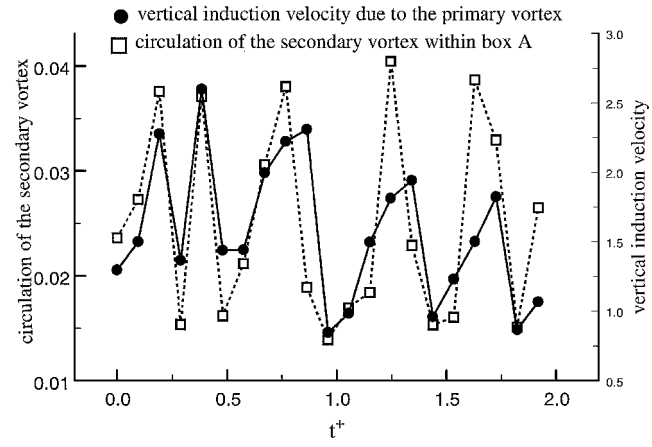

Fig. 3 Correlation between the vertical induction velocity caused by the primary vortex and the circulation of the secondary vorticity measured inside box A.

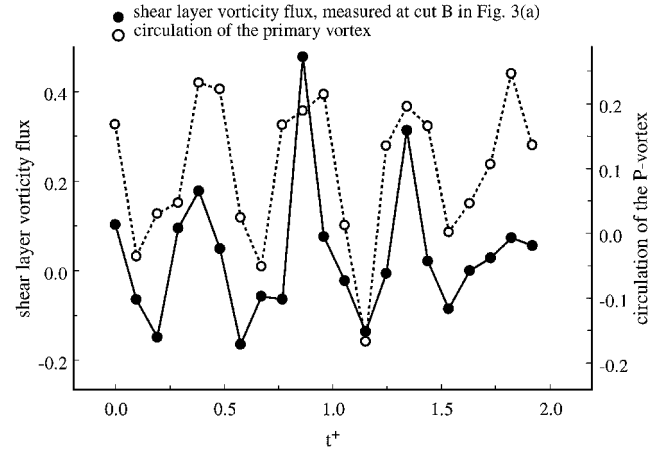

Fig. 4 Correlation between the shear-layer vorticity flux measured along cut B and the circulation of the primary vortex.

Primary Vortex Induction/Secondary Vortex Ejection

Based on the instantaneous vorticity fields, it appears that the induction imposed by the primary vortex on the secondary vortex is responsible for the ejection of the secondary vortex (Fig. 2a). This process can be examined by correlating the uplifting motion of the secondary vortex to the vertical induction velocity imposed on it by the primary vortex. To quantify the ejection process of the secondary vortex, a control volume (box A, as shown in Fig. 1) is selected to enclose a region directly above the time-averaged position of the secondary vortex. It is expected that the secondary vortex will move in and out of this control volume at different stages of the vorticity ejection process, that is, it will penetrate into this volume when ejected upwards, and exiting when the ejection subsides. Thus, the fluctuation of the total negative circulation inside the control volume can be used as a good indicator to characterize the ejection process. On the other hand, the upward-lifting velocity of the secondary vortex induced by the primary vortex can be estimated by using the Biot–Savart (B-S) rule. According to the B-S rule, the induction velocity caused by a simple line vortex is $|u_{\text{ind}}| = \Gamma/2\pi r$, where Γ is the total circulation of the vortex and r is the distance between the point of interest and the line vortex. First, we assume that the primary vortex can be represented by a collection of discrete vortical eddies, each with a concentrated vorticity $\omega_{i,j}$ that is located at (x_i, y_j). Second, the induction produced by the primary vortex is assumed to be acting only on the centroid of the averaged secondary vortex located at $(x_{\text{sc}}, y_{\text{sc}})$, which is determined experimentally. Finally, based on the preceding assumptions and the B-S rule, the induction velocity can be simplified as

$$\boldsymbol{u}_{\text{ind}} = \sum_{i,j} \frac{1}{2\pi}\left(\frac{\boldsymbol{\omega}_{i,j} \times \boldsymbol{r}_{i,j}}{|\boldsymbol{r}_{i,j}|^2}\right)\Delta x_i \Delta y_j$$

where $|\boldsymbol{r}_{i,j}| = \sqrt{[(x_i - x_{\text{sc}})^2 + (y_j - y_{\text{sc}})^2]}$. That is, the total induction on the secondary vortex is the sum of contributions from each discrete vortical eddy within the primary vortex. Figure 3 shows the time history of the induction velocity caused by the primary vortex and the circulation of the secondary vortex within the control volume (box A in Fig. 1). It is clear that there is a strong correlation between these two events, supporting our earlier assumption that the ejection of the secondary vortex is a result of the induction of the primary vortex.

Effect of the Ejection Process on the Primary Vortex

One direct consequence of the secondary vortex ejection is that the linkage between the rolling-up shear layer and the primary vortex is cut off (Fig. 2b). As a result, the feeding of vorticity from the shear layer to the primary vortex is interrupted. The strength of the primary vortex is determined by a balance between the constant feeding of vorticity from the shear layer and the continuous downstream transportation of vorticity through its vortex core. A disruption of the vorticity feeding will result in the subsequent weakening of the primary vortex. To obtain a reasonable estimate of the vorticity transportation from the shear layer into the primary vortex, we evaluate the vorticity flux $\int u\omega \, dy$ at a junction between the primary vortex and the shear layer. The junction is selected as the line that separates the shear layer from the primary vortex (cut B in Fig. 1). The selection of the line is subjective; however, the vorticity flux calculated is relatively insensitive to the choice of the line. The time variation of the feeding rate of the shear layer vorticity flux as defined is then compared with the total circulation of the primary vortex in Fig. 4. Both values show a quasi-periodic variation, and there is an excellent correlation between them. This clearly indicates that there is a direct influence of the vorticity feeding from the shear layer on the strength of the

primary vortex. As expected, increase/decrease of the feeding rate of the shear-layer vorticity leads directly to the enhancing/weakening of the primary vortex, respectively. Vorticity from the secondary vortex can be carried into the primary vortex as indicated by the presence of low-level counterclockwise vorticity in the primary vortex in the original PIV data. However, the entrained counterclockwise vorticity is relatively weak compared to the primary vorticity so it has not shown up in the interpolated vorticity data. Nevertheless, it can still play a role in weakening the primary vortex as suggested by Gordnier and Visbal[14] in their computational work.

Weakening of Both the Primary and the Secondary Vortices

The secondary vortex is significantly weakened after part of its vorticity is ejected from the surface. On the other hand, the weakening of the primary vortex results in the weakening of outboard-moving boundary-layer flow and this consequently hinders the recovery of the secondary vortex. In other words, one would expect that the feeding of vorticity into the secondary vortex would be related to the instantaneous variation of the total circulation of the primary vortex. Time variations of the circulation of the primary vortex and the vorticity flux of the secondary vortex are found to be strongly correlated (not shown here).

Reconnection of the Primary Vortex and the Shear Layer

The weakening of the primary vortex implies a smaller induction force on the secondary vortex. As a result, the secondary vortex settles back to the surface. In addition, the secondary vortex reduces in size and strength because of its ejection. The reduced influence of the secondary vortex allows the reconnection of the shear layer with the primary vortex, which in turn resumes the feeding of the shear-layer vorticity into the primary vortex. This event reenergizes the primary vortex, and a new cycle of the primary/secondary vortex interaction repeats.

It is clear from the preceding discussions that the primary/secondary vortex interaction process assumes a self-sustained manner. Once it is initiated, this interaction process no longer requires external perturbations to sustain it. At present, the exact triggering source for our experiments is not clear, although we suspect that inherent disturbances from the experimental setup (the vibration of the water towing tank facility) might be responsible, as another study[15] has suggested. Hubner and Komerath[16] have studied the quasi-periodic velocity fluctuations over a delta wing and showed the existence of fluctuating energy within a narrow frequency bandwidth. They further showed that the quasi-periodicity originated in the outboard region along the leading edge of the wing. This is consistent with the current observation that the interaction between the primary vortex and the secondary vortex occurs outboard near the leading edge.

Even in the absence of any inherent disturbances from the experimental setup, such ejection phenomenon has been observed in a numerical study.[5] Because the interaction is essentially self-sustained, it does not require any external excitations once it is initiated. Therefore, the interaction process can be considered as inherent and can be activated by many potential sources, such as the vibrations of the experimental setup, the interaction between the two primary vortices, the freestream and/or shear-layer disturbances, and the onset of vortex breakdown and wake instabilities.

Summary

The emphasis of our study is on understanding the vorticity dynamics and the unsteady characteristics of the delta-wing leading-edge vortices. Measurements taken on the crossflow planes reveal a self-sustained, quasi-periodic oscillation of the vortex system. Detailed analysis shows that the process is a direct result of a strong interaction between the primary vortex and the secondary vortex.

References

[1]Hall, M. G., "Vortex Breakdown," *Annual Review of Fluid Mechanics*, Vol. 4, 1972, pp. 195–218.

[2]Leibovich, S., "The Structure of Vortex Breakdown," *Annual Review of Fluid Mechanics*, Vol. 10, 1978, pp. 221–246.

[3]Escudier, M., "Vortex Breakdown: Observations and Explanations," *Progress in Aerospace Science*, Vol. 25, No. 2, 1988, pp. 189–229.

[4]Riley, A. J., and Lowson, M. V., "Development of a Three-Dimensional Free Shear Layer," *Journal of Fluid Mechanics*, Vol. 369, 1998, pp. 49–89.

[5]Cipolla, K. M., and Rockwell, D., "Small-Scale Vortical Structures in Crossflow Plane of a Rolling Delta Wing," *AIAA Journal*, Vol. 36, No. 12, 1998, pp. 2276–2278.

[6]Gursul, I., and Xie, W. S., "Buffeting Flows over Delta Wings," *AIAA Journal*, Vol. 37, No. 1, 1999, pp. 58–65.

[7]Ozgoren, M., Sahin, B., and Rockwell, D., "Vortex Structure on a Delta Wing at High Angle of Attack," *AIAA Journal*, Vol. 40, No. 2, 2002, pp. 285–292.

[8]Shih, C., and Ding, Z., "Unsteady Structure of Leading-Edge Vortex Flow over a Delta Wing," AIAA Paper 96-0664, Jan. 1996.

[9]Lin, J.-C., and Rockwell, D., "Transient Structure of Vortex Breakdown on a Delta Wing at High Angles of Attack," *AIAA Journal*, Vol. 33, No. 1, 1995, pp. 6–12.

[10]Visbal, M. R., "Origin of Computed Unsteadiness in the Shear Layer of Delta Wings," *Journal of Aircraft*, Vol. 32, No. 5, 1995, pp. 1146, 1147.

[11]Visbal, M. R., "Computational and Physical Aspects of Vortex Breakdown on Delta Wings," AIAA Paper 95-0585, Jan. 1995.

[12]Lourenco, L. M., Krothapalli, A., and Smith, C. A., "Particle Image Velocimeter," *Lecture Notes in Engineering*, edited by M. Gad-el-Hak, Vol. 45, Springer-Verlag, New York, 1989, pp. 127–199.

[13]Adrian, R. J., "Particle-Imaging Techniques for Experimental Fluid Mechanics," *Annual Review of Fluid Mechanics*, Vol. 23, 1991, pp. 261–304.

[14]Gordnier, R. E., and Visbal, M. R., "Unsteady Vortex Structure over a Delta Wing," *Journal of Aircraft*, Vol. 31, No. 1, 1994, pp. 243–248.

[15]Washburn, A. E., and Visser, K. D., "Evolution of Vortical Structures in the Shear Layer of Delta Wings," AIAA Paper 94-2317, June 1994.

[16]Hubner, J. P., and Komerath, N. M., "Spectral Mapping of Quasiperiodic Structures in a Vortex Flow," *Journal of Aircraft*, Vol. 32, No. 3, 1995, pp. 493–500.

J. C. Hermanson
Associate Editor

Numerical Study of N-Wave Propagation Using Optimized Compact Finite Difference Schemes

In Bo Shim,* Jae Wook Kim,† and Duck Joo Lee‡
Korea Advanced Institute of Science and Technology, Daejeon 305-701, Republic of Korea

Introduction

AMONG the aircraft noise sources, the fan is a dominant one in the high-bypass engine, especially during takeoff and landing. The fan noise can be classified into three types: blade passage frequency (BPF) tonal noise, multiple pure tonal (MPT) noise, and broadband noise. MPT noise levels can exceed the BPF tonal noise during takeoff and landing because shock waves are generated at the rotor tip in the today's high-bypass engine when the revolutions per minute of the engine shaft is increased to get maximum thrust.

Hawkings[1] analyzed the shock wave coalescence by using one-dimensional saw-toothed shock models. His analysis describes how an initial nonuniform wave train evolves to become increasingly irregular with distance. However, this type of analysis cannot be directly related to the irregularities in the fan geometry. The drawback

Received 21 March 2002; revision received 30 September 2002; accepted for publication 31 October 2002.

*Graduate Student, Department of Aerospace Engineering, 373-1 Kuseong-dong, Yuseong-gu; ibshim@acoustic.kaist.ac.kr.

†BK21 Research Professor, Department of Aerospace Engineering, 373-1 Kuseong-dong, Yuseong-gu; jwkim@acoustic.kaist.ac.kr.

‡Professor, Department of Aerospace Engineering, 373-1 Kuseong-dong, Yuseong-gu; djlee@mail.kaist.ac.kr. Member AIAA.